Supplementary material for Experimental implementation of assisted quantum adiabatic passage in a single spin

Jingfu Zhang[1], Jeong Hyun Shim[1], Ingo Niemeyer[1], T. Taniguchi[2], T. Teraji[2], H. Abe[3], S. Onoda[3], T. Yamamoto[3], T. Ohshima[3], J. Isoya[4] and Dieter Suter[1]

[1]Fakultät Physik, Technische Universität Dortmund, D-44221 Dortmund, Germany

[2]National Institute for Materials Science, 1-1 Namiki, Tsukuba, Ibaraki, 305-0044 Japan

[3]Japan Atomic Energy Agency, 1233 Watanuki, Takasaki, Gunma, 370-1292 Japan

[4]Research Center for Knowledge Communities,
University of Tsukuba, Tsukuba, 305-8550 Japan

(Dated: May 17, 2013)

PACS numbers:

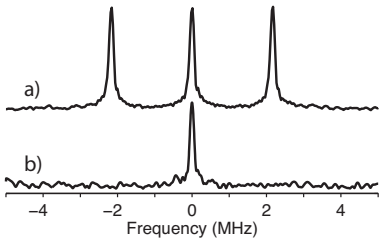

FIG. 1: Spectra of the NV electron spin obtained by a) hard and b) transition selective pulses.

I. SYSTEM AND SETUP

A. NV center system

The NV center used in the present study consists of an electron spin ($S = 1$) and a nitrogen- 14 nuclear spin (^{14}N with $I = 1$). Therefore, a state of the system can be represented in the basis of nine states, which can be written as $|m_S, m_I\rangle$. Due to the hyperfine interaction between the nuclear and electron spins, the frequencies of the three transitions indicated in Figure 1 a) are separated by about 2.1 MHz. To select a subspace of a two level system required to implement the assisted quantum adiabatic passage protocol, we reduced the amplitude of the microwave (MW) field to a value well below the hyperfine coupling constant, and precisely tuned the frequency to the center of the middle line. The spectrum obtained by the pulse with reduced power is shown in Figure 1 b). This selection allowed us to induce only the transition between $|m_S = 0, m_I = 0\rangle$ and $|m_S = +1, m_I = 0\rangle$ states, which span the subspace used in the present work.

In the experiment, we used a ^{12}C enriched diamond. The effect of a remote ^{13}C nuclear spin can be neglected here, and therefore we obtain long relaxation times, with $T_2^* > 100\,\mu$s. The sample used is a diamond single crystal grown at 5.5 GPa and 1400 °C. As a solid carbon source we used polycrystalline diamond plates synthesized by chemical vapor deposition (CVD) utilizing ^{12}C enriched methane [1]. According to the secondary ion mass spectroscopy analysis, ^{12}C enrichment of 99.995% was achieved in the grown crystals. The crystal was irradiated by 2 MeV electrons with a total fluence of 10^{11} e/cm^2 at room temperature and subsequently annealed at 1000 °C for 2 hours in vacuum.

B. Experimental setup

A single NV-center in diamond can be optically addressed using our home-built confocal microscope. For the optical excitation and detection of a single NV-center, a diode-pumped solid state continuous wave (CW) laser with 532 nm wave length was used. For pulsed experiments, an acousto-optical modulator with 58 dB extinction ratio and 40 ns rise-time generated the laser pulses from the CW laser.

We use a 4 GS/s arbitrary waveform generator (AWG) to synthesize the MW waveforms. The output of the AWG is then frequency up-converted at a double balanced mixer by mixing it with a stable frequency source (1 - 3 GHz). The lower sideband is filtered out by a properly selected band pass filter, which attenuates the upper sideband by 40 dB. The pulses are sent through an 8 W amplifier and a 20 μm copper wire attached to the diamond surface. Between individual runs lasting 3-4 hours, we calibrated the resonance frequency and microwave power to counteract drifts due to variations of the laboratory environment.

C. Laser and MW pulse sequences

In each approach, the first laser pulse initializes the spin into state $|0\rangle$. Then the MW pulse implements the AAP. The second laser pulse implements the measurement of the population of state $|0\rangle$. The fields in the two approaches are shown in Figure 4 in the main text, and for the rapid passage case, Figure 2 represents it for $b = 2$. The following section describes how the pulse shape is obtained.

II. PULSE SHAPES FOR THE RAPID-SCAN APPROACH

In the lab frame, the Hamiltonian for the mth segment with duration τ_m is

$$H_m(t) = -\omega_0 I_z - 2\omega_1 I_x \cos(\omega_m t + \phi_m), \tag{1}$$

where

$$t \in [\sum_{j=1}^{m-1} \tau_j, \sum_{j=1}^{m} \tau_j]. \tag{2}$$

Frequency ω_m and phase ϕ_m are constant during each segment.

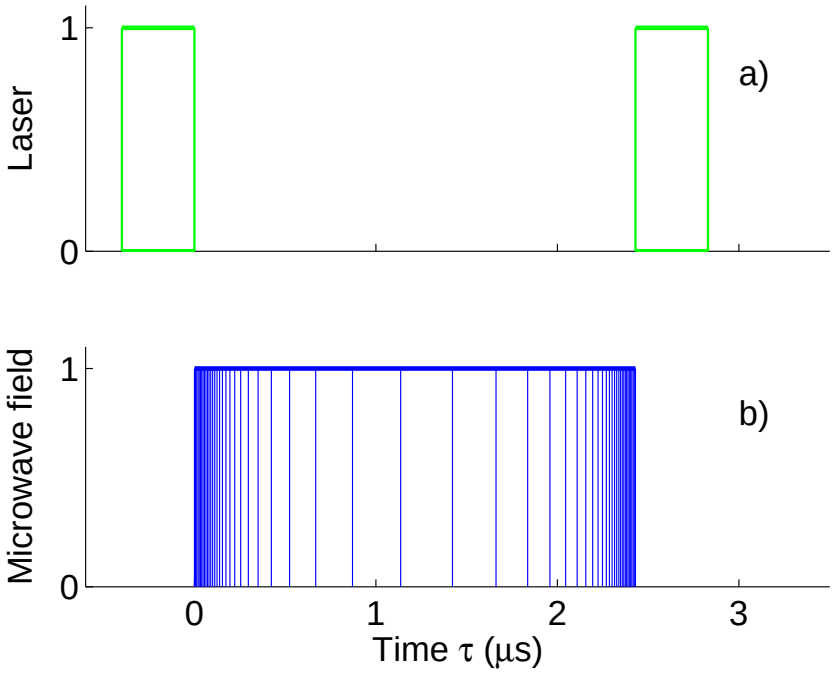

FIG. 2: Laser and MW pulse sequences for the case of $b = 2$ in the rapid-scan approach, shown as figures a-b), respectively, where amplitude of the microwave pulse takes the constant value Ω. The first laser pulse initializes the spin into state $|0\rangle$. The second pulse implements the measurement of the population of state $|0\rangle$. The duration of the laser pulses is 400 ns.

In the rotating frame, the effective Hamiltonian becomes

$$H_{m,eff} = -(\omega_0 - \omega_m)I_z - I_x\omega_1 \cos\phi_m + I_y\omega_1 \sin\phi_m. \tag{3}$$

We let

$$e^{-i\tau_m H_{m,eff}} = U_m \tag{4}$$

and therefore obtain

$$-(\omega_0 - \omega_m)\tau_m = \lambda(m\delta)\delta \tag{5}$$

$$-\omega_1\tau_m \cos\phi_m = \Delta\delta \tag{6}$$

$$\omega_1\tau_m \sin\phi_m = V_{CD}(m\delta)\delta. \tag{7}$$

By setting $\omega_1 = \Omega$, we obtain the parameters for the mth segment listed in the main text, and repeated here as

$$\tau_m = \delta\sqrt{\Delta^2 + V_{CD}^2(m\delta)}/\Omega. \tag{8}$$

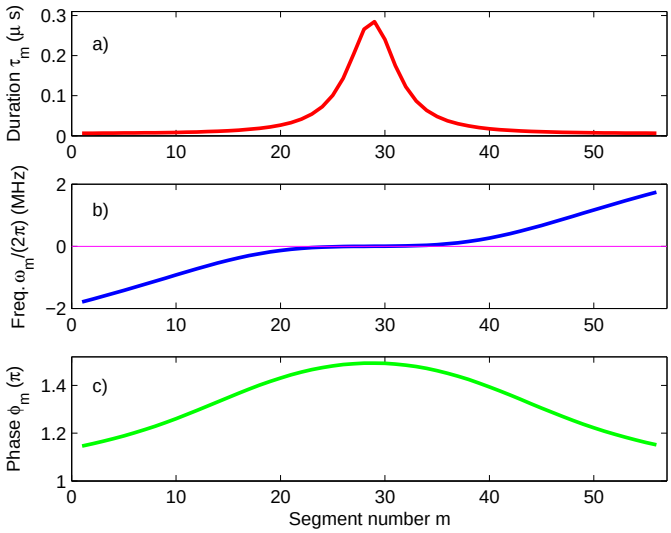

FIG. 3: The parameters of the pulses used in the rapid-scan approach when $b = 2$. Figures a-c) show the duration, carry frequency with respect to the transition frequency $\omega_0/(2\pi)$ and phase of the segment m.

$$\omega_m = \omega_0 + \delta\lambda(m\delta)/\tau_m \tag{9}$$

$$\tan\phi_m = -V_{CD}(m\delta)/\Delta. \tag{10}$$

Figure 3 shows the resulting values for these parameters for $b = 2$.

III. EXPERIMENTAL RESULTS AS 2D PLOTS

Figures 4 and 5 show the results represented in Figures 2 and 3 in the main text, in the form of 2-dimensional plots.

IV. OPTIMIZATION OF DRIVING FIELDS

Here, we investigate additional degrees of freedom for improving the fidelity of the scan or reducing its duration. For this purpose, we choose, instead of the linear time-dependence of the offset term considered in the main text,

$$\lambda(t) = \frac{b\sinh[c(t-1)]}{\sinh(c)} \tag{11}$$

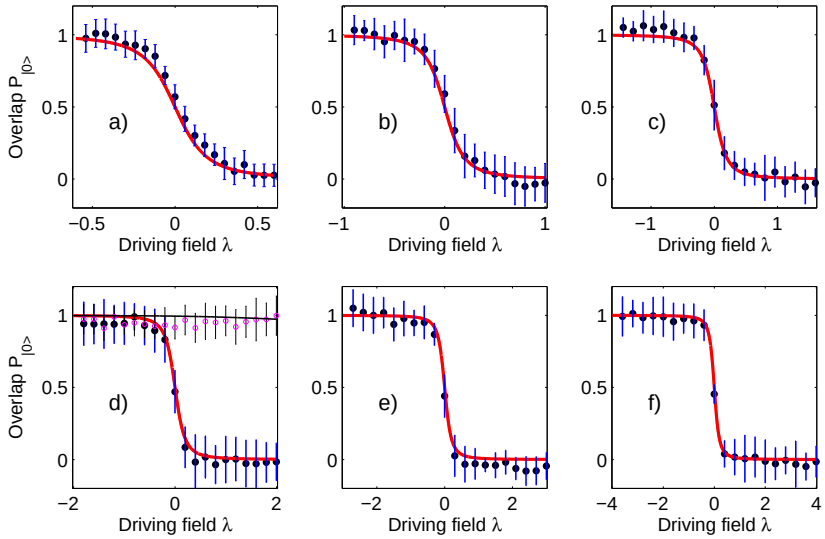

FIG. 4: (color online). The representation of Figure 2 in main text in 2 dimensional plots for the experimental results obtained with the analog implementation of the AAP. The individual experiments correspond to $b = 0.6$, 1, 1.6, 2, 3 and 4, shwon as figures a-f), respectively. The experimental data are shown as filled circles, and the corresponding error bars were obtained by repeating the experiment 10 times. The curves show the theoretical result for an ideal scan. In figure d) the empty circles with the almost horizontal line show the result for a reference experiment without CD field.

where $c > 0$ is a variable parameter that can be optimized. For $c \to 0$, we recover the linearly time dependent field that we studied in the main text:

$$\lambda(t) \to b(t-1) \tag{12}$$

Figure 6 illustrates the fields for $b = 2$, $c = 0.1$, 3.8 and 5, shown as figures a-c), respectively.

Our numerical simulation shows that the AAPs can be implemented. The loss of the fidelity due to time resolution in the analog approach is still vanishingly small, and can be completely neglected. Interestingly, in the rapid-scan approach, the maximal loss of the fidelity caused by digitalization is reduced. For example, the maximal loss (occurring at $\lambda = 0$) during the AAP is less than 5×10^{-4}. This appears to be the result of the slower passage of the driving field $\lambda(t)$ through the anti-crossing region, compared the linear case.

Figure 7 shows numerical results for the dependence of the scan duration on the parameter c. For each value of c, the required duration was determined by scaling the microwave

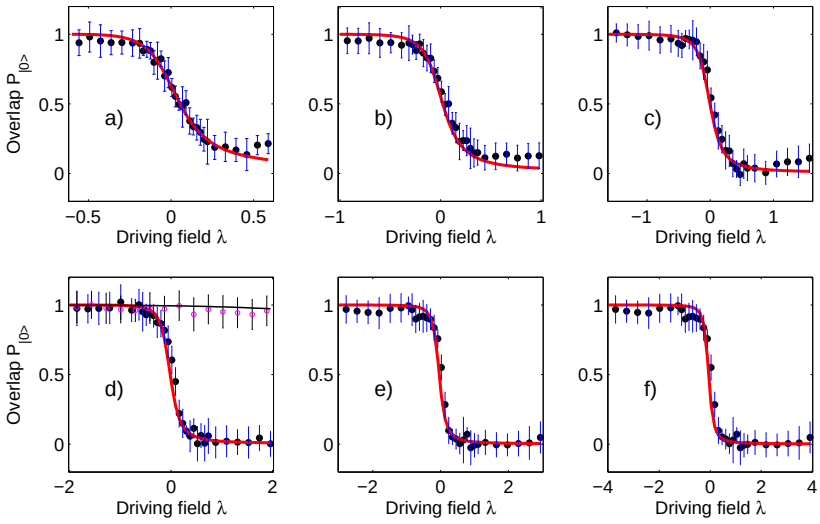

FIG. 5: (color online). The representation of Figure 3 in main text in 2 dimensional plots for Experimental results obtained with the rapid-scan approach. For details see the caption of Fig. 4.

amplitudes such that the maximum amplitude did not exceed 0.2 MHz. The duration of each time step was scaled accordingly. Apparently, the analog scan can be accelerated significantly in this approach. The optimum occurs at $c = 3.8$, where the duration becomes 3.4 μs, compared to the values 15.9 μs of the analog scan for $c = 0$ and 2.4 μs for the rapid-scan approach. Using this approach with more general functions, it should be possible to further reduce the scan duration.

[1] T. Teraji, T. Taniguchi, S. Koizumi, Y. Koide, and J. Isoya, Appl. Phy. Exp. **6**, 055601 (2013).

[2] J. Phys. Chem. A, **107**, 9937 (2003).

[3] S. Vega and A. Pines, J. Chem. Phys. **66**, 5624 (1977).

[4] L. M. K. Vandersypen and I. L. Chuang, Rev. Mod. Phys. **76**, 1037 (2004).

[5] C.P. Slichter, *Principle of Magnetic Resonance*, Springer-Verlag, Heidelberg.

[6] N. V. Vitanov, L. P. Yatsenko, and K. Bergmann, Phys. Rev. A **68**, 043401 (2003).

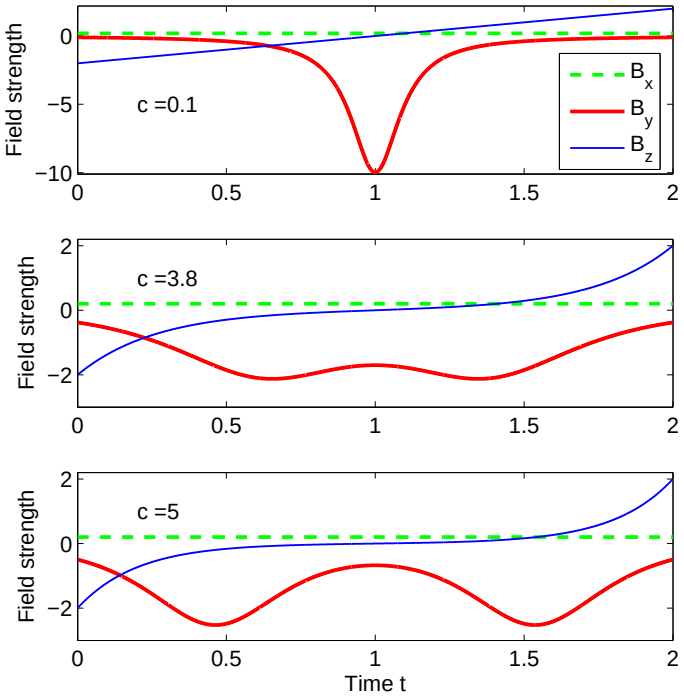

FIG. 6: (color online). Fields corresponding to $c = 0.1$, 3.8 and 5 in Eq. (11).

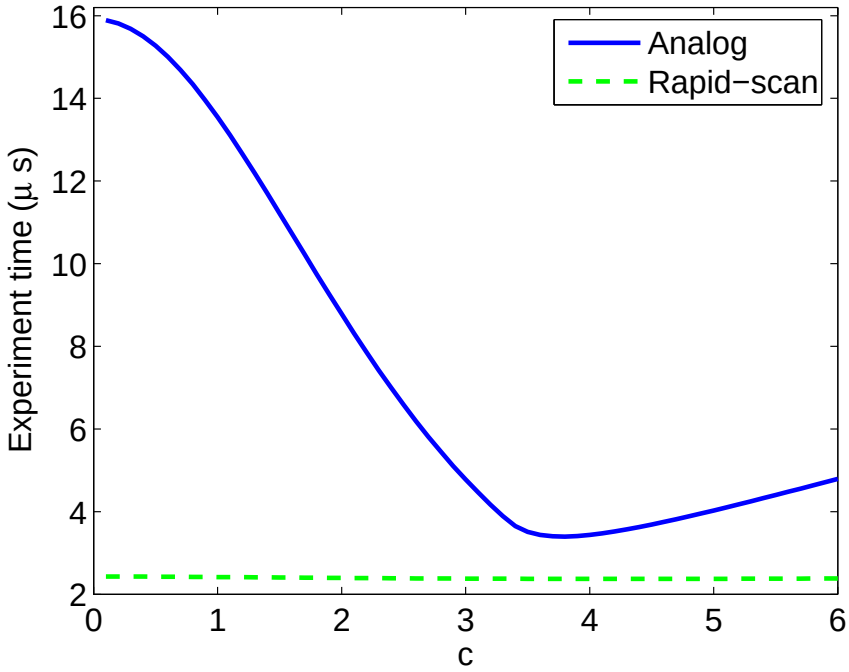

FIG. 7: (color online). Dependence of the experiment time on factor c in Eq. (11). The thick solid and dashed curves shows the time varying with c. One can find that there is an optimal c around 3.8 in the analog approach. The time in the rapid-scan approach does not change much.